Auger decay and subsequent fragmentation pathways of ethylene following *K*-shell ionization

B. Gaire,[1] D. J. Haxton,[2] F. P. Sturm,[1,3] J. Williams,[4] A. Gatton,[4] I. Bocharova,[1] N. Gehrken,[1,3] M. Schöffler,[3] H. Gassert,[3] S. Zeller,[3] J. Voigtsberger,[3] T. Jahnke,[3] M. Zohrabi,[5] D. Reedy,[4] C. Nook,[4] A. L. Landers,[4] A. Belkacem,[1] C. L. Cocke,[5] I. Ben-Itzhak,[5] R. Dörner,[3] and Th. Weber[1]

[1]*Chemical Sciences Division, Lawrence Berkeley National Laboratory, Berkeley, California 94720, USA*

[2]*Chemical Sciences Division and Ultrafast X-Ray Science Laboratory, Lawrence Berkeley National Laboratory, Berkeley, California 94720, USA*

[3]*Institut für Kernphysik, Goethe-Universität, Max-von-Laue-Straße 1, 60438 Frankfurt am Main, Germany*

[4]*Department of Physics, Auburn University, Alabama 36849, USA*

[5]*J. R. Macdonald Laboratory, Department of Physics, Kansas State University, Manhattan, Kansas 66506, USA*

(Received 19 May 2015; published 13 July 2015)

The fragmentation pathways and dynamics of ethylene molecules after core ionization are explored using coincident measurements of the Auger electron and fragment ions by employing the cold target recoil-ion momentum spectroscopy method. The influence of several factors on the dynamics and kinematics of the dissociation is studied. These include propensity rules, ionization mechanisms, symmetry of the orbitals from which the Auger electrons originate, multiple scattering, conical intersections, interference, and possible core-hole localization for the double ionization of this polyatomic molecule. Energy correlation maps allow probing the multidimensional potential energy surfaces and, in combination with our multiconfiguration self-consistent field calculations, identifying the populated electronic states of the dissociating dication. The measured angular distributions of the Auger electrons in the molecular frame further support and augment these assignments. The deprotonation and molecular hydrogen ion elimination channels show a nearly isotropic Auger electron angular distribution with a small elongation along the direction perpendicular to the molecular axis. For the symmetric breakup the angular distributions show a clear influence of multiple scattering on the outgoing electrons. The lowest kinetic energy release feature of the symmetric breakup channel displays a fingerprint of entangled Auger and photoelectron motion in the angular emission pattern identifying this transition as an excellent candidate to probe core-hole localization at a conical intersection of a polyatomic molecule.

DOI: 10.1103/PhysRevA.92.013408 PACS number(s): 33.80.Eh, 33.90.+h

I. INTRODUCTION

The emission of two electrons from a target atom or molecule following single-photon absorption depends on many factors (see, for example, [1] and references therein). For instance, such aspects are electron-electron correlation and entanglement [2–4], selection rules [5–7], ionization mechanisms [8–10], scattering and interference effects, and photon energy and polarization [11]. These characteristics dictate the kinetic energy and the emission pattern of the electrons escaping upon ionization of the target. The investigation of the photo–double ionization (PDI) of molecules by absorption of a single photon is hereby most challenging because of the additional inherent degrees of freedom and complex dissociation dynamics. Examples for this are the orientation of the molecular axis with respect to the polarization vector of the incoming light, the bond length, vibrational and rotational states involved, and the different fragmentation channels of the intermediate dication.

Following the detailed investigations of small diatomic molecules in the past as, for example, H_2 [12–14], N_2 [5,15,16], CO [17], and O_2 [18–20], attention has been turned to more complex systems such as CO_2 [21–24], H_2O [25,26], CH_4 [27,28], and C_2H_2 and C_2H_4 [29]. A polyatomic molecule can additionally disperse energy between its constituents at conical intersections on the potential energy surfaces (PESs), undergo conformation changes (such as isomerization or twisting), and its fragments can be electronically and vibrationally excited (see, for example, [29–33]). In recent experimental studies on the valence ionization of ethylene it was found that the single-step direct double ionization is most prominent (about 80% [29]) while a two-step process such as autoionization plays a minor role. In the *K*-shell ionization studied in this work, however, the situation is much different; the two-step processes of photoionization followed by Auger decay will dominate.

Ethylene (C_2H_4) is the simplest hydrocarbon molecule with a double bond. The electronic configuration of neutral ethylene is $1a_g^2\,1b_{1u}^2\,2a_g^2 2b_{1u}^2 1b_{2u}^2 3a_g^2 1b_{3g}^2 1b_{3u}^2$ in the D_{2h} symmetry group [31,34] with $1a_g^2$ and $1b_{1u}^2$ representing the carbon $1s$ type orbital. The threshold energy required for the carbon $1s$ ionization in ethylene is 290.8 eV [35,36] with an energy splitting of only 0.02 eV between gerade and ungerade states [37]. The orbitals $2a_g^2$, $2b_{1u}^2\,1b_{2u}^2$, $3a_g^2$, and $1b_{3g}^2$ are referred to as inner valence orbitals and are of σ type. The $1b_{3u}^2$ orbital is the highest occupied molecular orbital (HOMO) of π type and mostly referred to as a valence (or outer valence) orbital. In addition to these occupied orbitals there are unoccupied virtual orbitals, namely, $1b_{2g}3b_{1u}2b_{2u}4a_g2b_{1u}2b_{3g}$, which also play a role in Auger decay. Here the $1b_{2g}$ orbital represents the lowest unoccupied molecular orbital (LUMO) of π^* type. The $3b_{1u}$, $2b_{2u}$, $4a_g$, and $2b_{3g}$ orbitals are of σ type [34].

The absorption of a photon with energy above the double ionization threshold can lead to an ejection of an inner-shell electron. The hole will then be filled by a valence electron. While doing so, another valance electron is set free and this electron is referred to as an Auger electron. This transition can

be described as $(n''l''j'') \rightarrow (nlj)(n'l'j')$ where the electrons are represented by the quantum numbers nlj, where n is the principal quantum number, l is the orbital angular momentum quantum number, and j is the vector sum of l and the spin quantum number s. The kinetic energy of the Auger electron, denoted with E_{Auger}, is given by $E_{Auger} = E_{n''l''j''} - E_{nlj,n'l'j'}$, where $E_{n''l''j''}$ is the energy of the level with a hole (quantum numbers $n''l''j''$) and $E_{nlj,n'l'j'}$ is the energy of the final vacant levels (these energies are taken with respect to the energy of the neutral state of the atom or molecule) from where the "down" electron (i.e., the electron filling the hole and the quantum numbers of the final vacancy $n'l'j'$) and the Auger electron (i.e., the subsequently emitted electron with quantum numbers of the final vacancy nlj) originate, respectively [38].

There are at least three possibilities of Auger decay pathways leading to the measured Auger electron energies in our experiment. One is the direct or normal Auger process (DA); in this case the carbon $1s$ electron is ejected by the incident photon creating a hole in the K shell. This hole is then filled by a valence electron and at the same time an outer valence electron is ejected into the continuum. The second possibility involves the satellite states (SA) in which the ionization from the carbon $1s$ is accompanied by an electron excitation from the bound π state (i.e., HOMO) to the π^* state (LUMO), also referred to as $\pi-\pi^*$ shake-up satellite [39]. When the hole in the $1s$ shell is filled by a valence electron the π^* electron is ejected as an Auger electron. The third mechanism is similar to the conjugate process (CA), i.e., a carbon $1s$ electron is excited to the LUMO π^* state (or to another neighboring virtual orbital), while an outer valence electron is ejected as a photoelectron. The hole in the $1s$ orbital is then filled by a valence electron knocking the resonantly excited π^* electron (or the one from the other virtual orbital) to the continuum; this results in an Auger electron with a kinetic energy higher than that from the direct Auger process.

For all these pathways double ionization involving Auger decay is thought of as a process with two independent steps involving electrons from different shells [40]. For K-shell ionization near threshold the kinetic energies of these two outgoing electrons are usually very different (about 10 eV for slow photoelectrons and above 100 eV for fast Auger electrons) and therefore these electrons can be very well distinguished in an experiment. The Auger electron emission is a very fast (<10 fs) process and hence the geometry typically does not have much time to adjust to the loss of the photoelectron. Accordingly, the following questions arise: What is the significance of (i) electron-electron correlation or entanglement on the Auger electron angular emission pattern and, moreover, (ii) how does the ionic breakup depend on the Auger decay and vice versa? One would assume that the former must be rather small since Auger decay is mostly an intershell process. The latter on the other hand is thought of as having a big influence in core-hole localization [41] but also may be rather subtle for homonuclear molecules; however, it has just been shown in photofragmentation of C_2H_2 that the isomerization process starts very early in the Auger decay; in fact it begins right within the Franck-Condon region of the transition [42]. Moreover, given the high Auger electron kinetic energy, and thus a wavelength in the order of the distance between the atomic constituents, multiple scattering and interference effects of the Auger electrons are expected to be sensitive to the molecular structure [43,44], which dissociates into two or more fragments.

After the Auger decay the molecule is at least doubly ionized and hence fragmentation into different channels is possible. Because of the high electron energy and the multitude of energy levels involved, it is very hard to treat molecular Auger decay theoretically. It is up to experiments to find out which states play a role and which properties, i.e., electron-electron correlation, entanglement, localization, fragmentation pathways, electron scattering, etc., need to be taken into account. In the present study we are using ethylene to investigate if the fragmentation pathways following the Auger decay are different from those following valence PDI, and if electron-electron correlation or entanglement plays a role. Ethylene is a centrosymmetric molecule with a C=C double bond and therefore the K-shell ionization will not directly allow for observing effects based on core-hole localization unless the photoelectron is measured in coincidence with the Auger electron as described further below. However, it will allow us to cleanly test the influence of the Auger decay on the subsequent molecular fragmentation and its kinematics by comparing symmetric and asymmetric breakup channels. One reason why one might expect the fragmentation of the doubly ionized species, which are produced by the inner-shell ionization followed by the Auger decay, to be different from the valance PDI is that there are some propensity rules which favor the population of certain types of states, depending on the ionization mechanism and the geometry of the molecule. For closed-shell centrosymmetric molecules (for example, ethylene) triplet gerade and singlet ungerade states are favored in the PDI [5–7], while mostly singlet states are populated in the core ionization followed by the Auger decay [45,46]. Selection rules may prevent small contributions from triplet states to be visible. In order to find out if triplet states need to be considered in the K-shell ionization, we chose circularly polarized light to avoid many selection rules (caused by the photoabsorption) from influencing the electron emission pattern.

In this work we explore the energy correlation maps of ethylene fragmentation after Auger decay in addition to the angular distribution of the Auger electrons that are measured in coincidence with the recoiling ions of the subsequent Coulomb explosion. The measured kinetic energies of the ions and Auger electrons help us to identify the ionization mechanisms and the set of electronic states of the dissociating dications that are populated and eventually lead to specific states of the fragments in the particular dissociation limits. The electronic dication states observed describe the doubly charged molecular ion after the core hole was filled, an Auger electron was emitted, and consequently two vacancies were left behind in the valence shells before the breakup of the molecule took place. The molecular frame Auger electron angular distributions (MFAADs) provide further support to the state assignments as the angular distributions are often indicative of the orbitals from which the Auger electrons are ejected [47,48] and sometimes reveal entangled electron pairs (as in Ref. [4]).

II. EXPERIMENTAL METHOD

This experiment was performed at beamline 11.0.2 of the Advanced Light Source at the Lawrence Berkeley National Laboratory by employing the cold target recoil-ion momentum spectroscopy (COLTRIMS) method [49–51]. Right circularly polarized photons with energy of 310 eV intersected a supersonic gas jet of internally cold ethylene molecules (∼80 K) at a right angle inside the momentum spectrometer. The ionization process resulted in a photoelectron, an Auger electron, and two positively charged Coulomb exploding fragments. In this experiment we only measured the Auger electron and the fragment ions in coincidence. This configuration was chosen to ensure good energy resolution (about ±0.5−2 eV) and angular resolution (approximately ±3°) for the Auger electrons. Such measurements are challenging for momentum imaging systems such as COLTRIMS because the Auger electrons have high kinetic energy (a few hundred eV) and hence had to be decelerated by applying a retarding field. The spectrometer is similar to the one used in Refs. [47,51]. The retarding field, however, leads to the rejection of low-energy electrons including the photoelectrons from reaching the detector. Only the Auger electrons within a cone of about 15° along the spectrometer axis were recorded, while for the recoiling ions the full collection angle of 4π (sr) was retained on the detector in the opposite arm of the three-dimensional (3D) momentum spectrometer. The data were recorded in list mode and processed in an intricate offline analysis. The 3D-momentum vectors of the ions and electrons were measured by recording the time-of-flight (TOF) to and the position of impact on the specific particle detectors located at the opposite ends of the spectrometer. From the 3D-momentum vectors we deduced the respective kinetic energy and the angular distribution of the particles. Subsequent transformations of the coordinate systems enabled us to generate the desired MFAADs. The kinetic energy release (KER) of the fragment ions was derived from the motion in the center-of-mass frame of the molecule and the KER resolution was approximately ±0.1 eV.

III. RESULTS AND DISCUSSION

For channels with two fragment ions (i.e., dissociative ionization) the photoion-photoion coincidence (PIPICO) spectrum, i.e., a yield plot of the TOF of the first fragment ion as a function of the TOF of the other ion, is used to distinguish the different breakup channels which show up as separate stripes in the graph (not shown here; see Refs. [16,29] as examples). The following channels are observed from the interaction of the $E_\gamma = 310$ eV right circularly polarized photons with the ethylene molecule:

$$
\begin{aligned}
&C_2H_4 + E_\gamma \rightarrow {C_2H_4}^{2+} + e_P^- + e_A^- && \text{nondissociative,}\\
&C_2H_4 + E_\gamma \rightarrow H^+ + {C_2H_3}^+ + e_P^- + e_A^- \\
&C_2H_4 + E_\gamma \rightarrow {CH_2}^+ + {CH_2}^+ + e_P^- + e_A^- && \text{dissociative,}\\
&C_2H_4 + E_\gamma \rightarrow {H_2}^+ + {C_2H_2}^+ + e_P^- + e_A^-
\end{aligned}
$$

where E_γ is the photon energy, e_P^- is the photoelectron, and e_A^- is the Auger electron. These channels are separated by taking advantage of the position of impact on the detector and TOF information of the ions measured. In the static electric field of the spectrometer lighter ions (smaller mass to charge ratio) have shorter flight times to the detector. In addition, the ions with lower energy have a narrower spread in their position distribution. For example, the long-lived dications (${C_2H_4}^{2+}$) have almost no spread in their position and a sharp TOF distribution, compared to the fragment ions which show much broader distributions in time and position (e.g., ${CH_2}^+$ with a similar mass to charge ratio to ${C_2H_4}^{2+}$) due to their breakup energy [29]. The branching ratios of all these channels are given in Ref. [29]. However, our recent advanced analysis of this dataset revealed a dead spot on the ion detector influencing the breakup channels differently. The revised branching ratios are presented in Table I. The corrections can be considered minor as they are within the statistical error bars of our original results.

A. Energy maps

The energy correlation maps, i.e., the yield of fragmentation events as a function of the E_{Auger} and KER, are shown in Fig. 1 for three fragmentation channels. The wide range of E_{Auger} measured in our experiment (from about 250 to 268 eV) is an indication that all three different Auger decay mechanisms (i.e., DA, SA, and CA) introduced earlier play a role. Though we did not record photoelectrons in the current measurement, the kinetic energies of the photoelectrons from the K-shell ionization of ethylene molecules in a similar photon energy range are reported in the literature [52]. The reported photoelectron energy distribution in fact shows satellite lines in addition to the main line in Ref. [52]; however, in that experiment the corresponding Auger electrons were not recorded. From these yields and our branching ratios we can deduce that for 310-eV photons the DA mechanism is likely to dominate. The SA and CA mechanisms are less probable and likely contribute on a comparable level (they are hard to distinguish in [52] as they fall in the similar kinetic energy range of the photoelectron).

The signature to clearly identify all these processes would be to measure the characteristic energy sharing between the different Auger- and photoelectrons for each respective fragmentation channel. Unfortunately, with our current setup we could only record the Auger electron in coincidence with the ionic fragments. However, this enables us to probe the PESs of the dication in so-called energy correlation maps in greater detail.

The E_{Auger} distribution for the main feature of the deprotonation ($H^+ + {C_2H_3}^+$) channel [indicated as (I) in Fig. 1(a)] has a peak at about 257 eV. The main peak position decreases to 254 eV for the symmetric breakup (${CH_2}^+ + {CH_2}^+$) channel

TABLE I. Auger electron kinetic energy (E_{Auger}), kinetic energy release (KER), and the branching ratio (sum over all channels is 100%) of the different breakup channels from the Auger decay of C_2H_4. The features are labeled (I–IV) in Fig. 1 to help the reader follow the discussion.

Channels	Feature (See Fig. 1)	E_{Auger} (eV)	KER (eV)	Branching ratio (%)
$C_2H_4^{2+}$	—	260	—	5.4 ± 1.1
$H^+ + C_2H_3^+$	Main (I)	257.5	4.5	46.7 ± 8.5
	Minor (II)	265	4.5	3.6 ± 0.7
$CH_2^+ + CH_2^+$	Main (I)	254	5.9	37.6 ± 6.8
	Minor (II)	261	5.9	2.7 ± 0.5
	Island (III)	258	4.2	2.2 ± 0.4
$H_2^+ + C_2H_2^+$	Main (I)	253	4.6	1.2 ± 0.2
	Minor (II)	262	4.6	0.6 ± 0.1

[island (I) in Fig. 1(b)] and it is even lower for the molecular hydrogen ion elimination ($H_2^+ + C_2H_2^+$) channel [island (I) in Fig. 1(c)], which shows a peak value of about 253 eV. This trend already indicates that different electronic states of the dication are responsible for the three different breakup channels. Consequently, one can expect different Auger electron angular distributions for these channels, which will be presented further below (Sec. III B).

While examining the cuts of the PESs depicted in Fig. 2(a) (from [29]; note that only the singlet states are shown) the energetics from the energy correlation map in Fig. 1(a) reveal that the main feature of the deprotonation channel [island (I) with E_{Auger} peaking around 257 eV] is the result of populating the first electronically excited state (S_2) of the ethylene dication. From the center of the Franck-Condon region [arrow near the bottom in Fig. 2(a)] the dicationic population dissociates along the diabatic S_2 curve and at around a C-H distance of 5 bohrs transfers to the diabatic limit of the S_3 state. The expected KER is the difference of the barrier energy at about 33 eV (which is at the crossing of the S_2 and S_3 state around a C-H distance of 5 bohrs) and the asymptotic limit of 28.4 eV. This expected KER of 4.6 eV is in reasonable agreement with our measured value of 4.2 eV. An alternative path on the PES of this feature of the deprotonation channel can be initiated by populating the S_3 state, which then dissociates to the diabatic S_2 limit (KER of 4.4 eV) and less likely to the S_3 limit (KER of 5.6 eV), resulting in a small tail of the KER distribution shown in Fig. 1(a) [island (I)]. The relatively narrow KER distribution measured in our experiments indicates that not many pathways, other than those suggested here, are contributing.

In the case of the symmetric breakup channel ($CH_2^+ + CH_2^+$) the KER distribution for the main feature peaks around $E_{\text{Auger}} = 254$ eV [island (I) in Fig. 1(b)] and is clearly broader than that of the deprotonation channel. The possible dissociation pathways for this feature in Fig. 2(b) proceed via the $^1B_{3u}$ state to the dissociation limit marked as B (expected KER is $35 - 29.6 = 5.4$ eV) and the excited

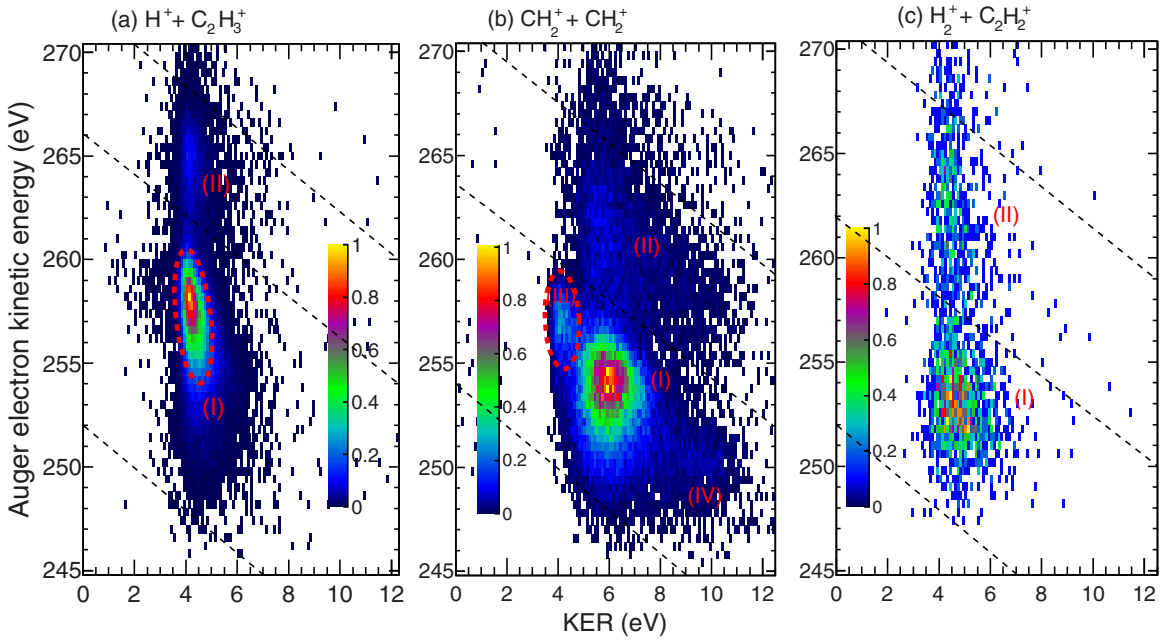

FIG. 1. (Color online) Density plots of the kinetic energy release (KER) and Auger electron kinetic energy (E_{Auger}) of the double ionization of C_2H_4 at 310 eV for (a) $H^+ + C_2H_3^+$, (b) $CH_2^+ + CH_2^+$, and (c) $H_2^+ + C_2H_2^+$ channels, respectively. The different features relevant to our discussion are labeled as (I)–(IV). The diagonal dashed lines represent the different energy regions for the Auger electron angular distributions presented in Figs. 4–7.

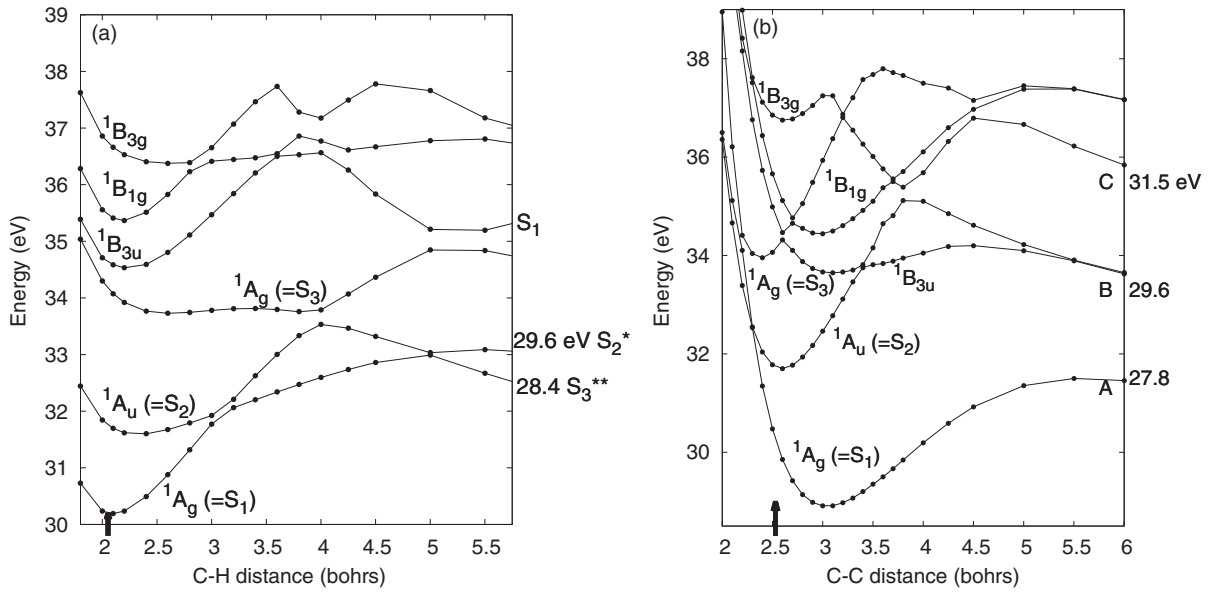

FIG. 2. Cut of the selected singlet potential energy surfaces (PESs) of the ethylene dication for the (a) C-H and (b) C-C distance calculated using the multiconfiguration self-consistent field method (adapted from Ref. [29]). The black arrows at the horizontal axis show the center of the Franck-Condon region.

vibrational levels of the $^1B_{1g}$ state to the same dissociation limit marked as B (expected KER is 35.5−29.6 = 5.9 eV). We also observe a diffuse island at a KER of about 9.6 eV and a corresponding Auger electron energy of about 250 eV [island (IV) in Fig. 1(b)]. These events appear to be due to a population of a higher-lying electronic singlet state (with a double ionization potential of around 39 eV, which is currently not covered by our calculations) that perhaps intersects with the $^1B_{3u}$ state and then dissociates to the limit marked as B in Fig. 2(b). The very low yield also suggests the less likely repulsive triplet state $^3B_{2g}$ (double ionization potential around 37.5 eV), which directly dissociates to the limit marked as A (see Ref. [29]), to be the source of this faint feature.

The islandlike feature in the energy map of the symmetric breakup channel in Fig. 1(b) [marked with an ellipse and labeled (III)] at very low KER is the result of populating the S_2 state. The S_2 state then dissociates to the limit marked as A [see Fig. 2(b)] via a conical intersection between S_2 and S_1 at around 2.3 bohrs (expected KER is 32.2−27.8 = 4.4 eV). It is worthwhile to stress that, as we described above, populating the S_2 state followed by dissociation along the C-H coordinate contributes to most of the deprotonation, which is also the most likely breakup channel. Clearly, the population of the S_2 state around the vertical energy of 33 eV in the Franck-Condon region finds an easier and faster path to dissociation along the C-H stretch instead of going through the complex dynamics via conical intersections to the S_1 state along the C-C coordinate. This is likely the reason why we observe very little dissociation along the C-C stretch resulting in the small islandlike feature in the symmetric breakup channel [island (III) in Fig. 1(b)].

The main feature in the energy map of the molecular hydrogen ion elimination channel ($H_2^+ + C_2H_2^+$) [island (I) in Fig. 1(c) with an E_{Auger} peak around 253 eV] is similar to the pathway found in the valence PDI study in Ref. [29]. In short, this pathway involves a concerted scissoring motion of the H-C-H bond angle towards smaller openings and a simultaneous stretch of the C−H_2 center-of-mass distance. While scissoring and stretching, the molecule finds a way via the conical intersection to a repulsive state and dissociates. In contrast to the valence PDI, the overall yield of this channel is reduced in the Auger decay because in general triplet states are less likely to be populated. Hence, the dissociation paths involving the triplet states are closed straightaway leaving $^1B_{2g}$, $^1B_{2u}$, ^1A_g (S_4), and $^1B_{1u}$ to be the most likely populated dication states in the Auger decay.

A minor feature with the same KER as the main feature is clearly visible in the energy correlation maps in Fig. 1 [islands (II)] of all three breakup channels (deprotonation, symmetric, and molecular hydrogen ion elimination). In the deprotonation channel the minor feature consists of a separate distinct peak in the Auger electron energy distribution (E_{Auger} around 265 eV). It is also a separate peak in the molecular hydrogen ion elimination channel (E_{Auger} around 262 eV). For the symmetric channel this feature appears as a shoulderlike distribution in the E_{Auger} distribution [i.e., a projection of Fig. 1(b) along the vertical axis, not shown here]. This in turn suggests that different states are involved for the production of these minor features [islands (II)] for the various breakup channels.

Theoretical results for the Auger electron energies of C_2H_4 can be found in Ref. [31]. On the experimental side Rye *et al.* [53] reported seven peaks in the Auger electron energy distribution, though these spectra are not for individual fragmentation channels and their features but are integrated over all possible ionization processes and fragmentation channels. At least three peaks in our measurement are close to the values reported in Ref. [53] (i.e., peaks at 266, 257, and 252.6 eV). Also two of the peaks (253 and 257 eV) from Ref. [54] are observed in our data. It is important to stress that, due to the chosen retarding electrical field in our setup, we

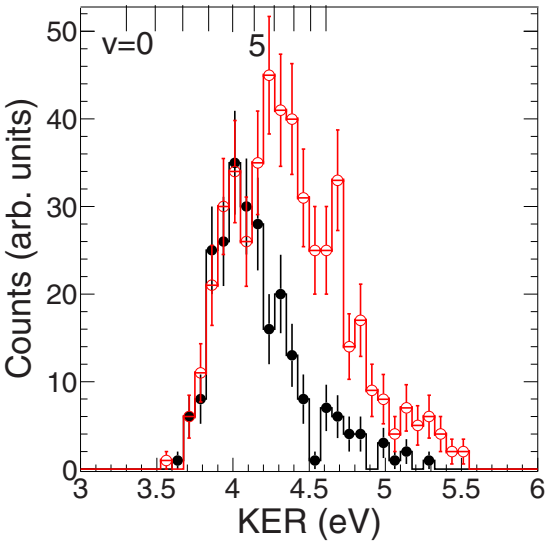

FIG. 3. (Color online) Vibrational level progression for the main feature of the $H^+ + C_2H_3{}^+$ channel. The KER distribution is shown for selected Auger electron energies E_{Auger} [solid black circles for $E_{\text{Auger}} = 259-260$ eV and open red circles for $E_{\text{Auger}} = 255-257$ eV energy range]. The vertical lines on the top axis represent the expected KER for the respective vibrational levels.

cannot detect any Auger electrons below kinetic energies of about 250 eV that may be produced.

In the following we concentrate on the main feature in the energy correlation map of the deprotonation channel [island (I) in Fig. 1(a)]. The KER distribution for selected Auger electron energies E_{Auger} is shown in Fig. 3. The structured KER distribution as displayed in Fig. 3 suggests a progression of vibrational bound states that dissociate by coupling to a repulsive curve. One can clearly see that for higher Auger electron energies E_{Auger} only one (or a few) vibrational level(s) is(are) dominant (solid black circles), while for low E_{Auger} the KER distribution gets broader, showing finer structures (open red circles), which likely stem from additional vibrational levels. The expected KER from these vibrational levels are marked on the top axis in Fig. 3. The energies of the vibrational levels are calculated using the phase amplitude method [55].

We conclude that we have identified some of the states and dissociation paths involved in the fragmentation channels based on the KER and the E_{Auger} as discussed above and mentioned in Ref. [29]. In the next subsection we investigate the molecular frame Auger electron angular distributions (MFAADs) to shed more light on the populated dicationic states, which lead to the here-identified dissociation pathways on the PESs.

B. Auger electron angular distribution

In this subsection we examine the measured MFAADs. For channels with fragments of different masses we choose the lighter ion going to the right. The molecular axis (horizontal) is defined by the two-body breakup of the molecule into two ionic fragments. We used circularly polarized light with the light propagation going into the figure plane (in Figs. 4–6). We select the ions and Auger electrons which are emitted at $90^\circ \pm 20^\circ$ to the light propagation and show the azimuthal angle of the Auger electron around the light propagation with zero being the direction of the lighter fragment ion. We discuss the Auger electron angular distributions of each channel beginning with the deprotonation.

1. $H^+ + C_2H_3{}^+$ *channel*

The Auger electron angular distribution of the deprotonation channel for the main feature [marked as (I) of Fig. 1(a)] in the energy correlation map ($252 < \text{KER} + E_{\text{Auger}} < 266$ eV) is shown in Fig. 4(a). The distribution is almost isotropic with a little more elongation perpendicular to the molecular axis. This may indicate that the decay leads preferentially to an emission of electrons from π orbitals. The most likely dication state for the deprotonation channel with a prominent contribution is the first excited singlet state S_2 $[1b_{3g}^{-1}, 1b_{3u}^{-1}]$, which results from the loss of electrons from σ and π orbitals, as identified from the measured energies above. The smaller contribution from the σ transition probably is from the excited singlet state S_3 ($[1b_{3g}^{-2}]$, i.e., a state with two electrons removed from a σ orbital).

The Auger electron angular distribution for the minor feature of the deprotonation [see island (II) in Fig. 1(a): $266 < \text{KER} + E_{\text{Auger}} < 272$ eV] is shown in Fig. 4(b) and seems to be dominated by an electron emission from π orbitals as well. Due to this emission pattern and the small yield observed here, these rare events are potentially associated with the less likely CA process that we have described earlier where the $1s$ electron has been excited to the virtual π^* orbital followed by an ejection of a valence electron. Subsequently, another valance electron filled the core hole while releasing the just created π^* electron as an Auger electron. However, a contribution from the rare SA mechanism including the shake-up satellite states cannot be ruled out as they also involve π electrons in the ionization and excitation process. In addition, during the K-shell ionization electrons can be excited to virtual σ-type orbitals either by CA or SA and then be ejected via the decay of inner valence electrons resulting in an Auger energy, which is less than that of the ionization of the π^* electron from the decay of the outer valence electron described above. The Auger electron energy from such a scenario is expected to be about 261−262 eV and is experimentally well reproduced in the minor feature of the symmetric channel and the molecular hydrogen ion elimination of Figs. 1(b) and 1(c) [islands (II); further discussed below in Secs. III B 2 and III B 3].

Clearly, within the statistical error bars, the MFAADs presented above do not show any distinct structure. A distinct structure could be caused by possible effects such as diffraction or core-hole localization. Such effects will be most prominent with respect to the C-C axis; however, if present, traces of that are expected to be visible in the deprotonation channel as well. No evidence of that is seen here although no significant conformation change such as isomerization is likely to occur during the short time of the Auger decay [19], which would cause the axial recoil approximation and hence the postselection of the molecular orientation in our analysis to fail. With the axial recoil approximation intact and the short

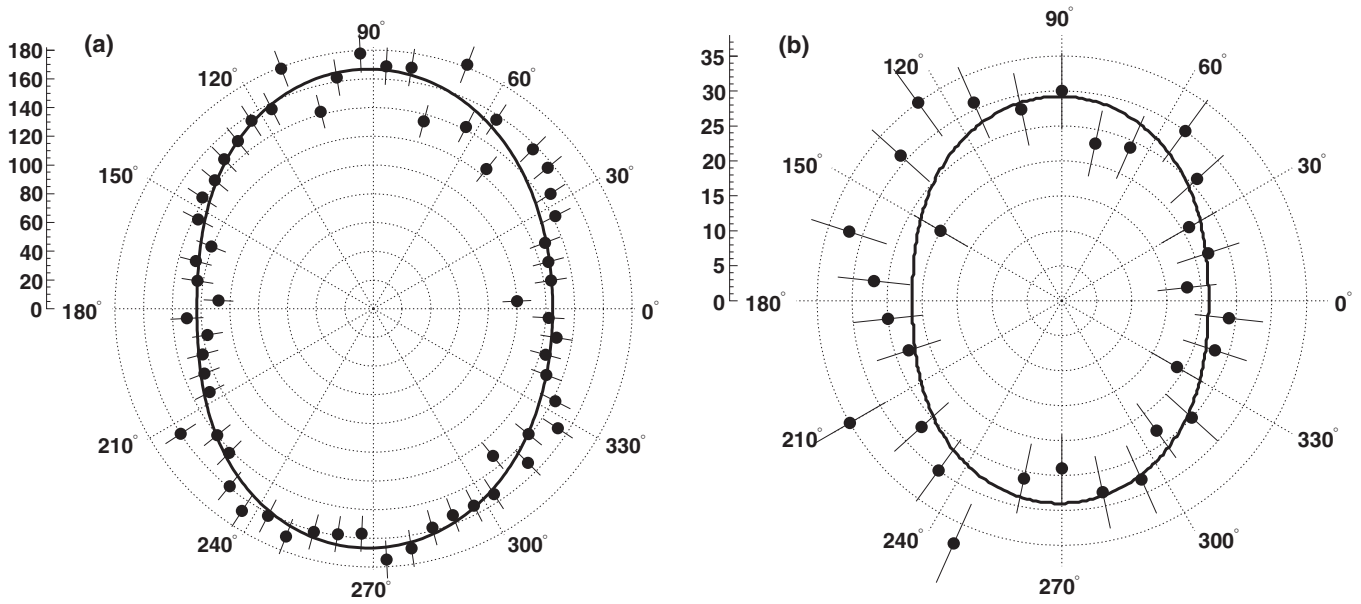

FIG. 4. Angular distribution of the Auger electrons in the molecular frame for the $H^+ + C_2H_3{}^+$ channel (a) for the main feature (I) and (b) for the minor feature (II) from the energy map in Fig. 1(a). The lines are the sum of spherical harmonics fitted to the measured data (using $l = 0, 1, 2$ and $m = 0$ only). The proton is going to the right and the plane of the figure represents the polarization plane of the circular polarized light.

wavelength of the Auger electron, diffraction is expected to take place. The diffraction could be caused by a superposition of multiple scattering waves of the outgoing electron (electron wavelength about 1.5 a.u.) in the molecular potential (C=C bond length about 2.4 a.u.). The absence of the diffraction pattern might be due to the fact that we do not know which proton was expelled. While it is most likely that one of the two protons, which were closest to the photoionized carbon atom, was separated, we cannot distinguish between these two candidates in our experiment. Thus our measurements likely represent a superposition of these two possible orientations causing an averaging effect in our MFAADs displayed in Fig. 4.

This lack of orientation would also influence possible effects of core-hole localization, at least around the axis of the asymmetric two-body breakup; however, a possible left-right asymmetry, i.e., a preferred emission along the direction of the heavy fragment (or vice versa), should still be visible if present. In general, an asymmetry in the angular distribution is possible once electrons with gerade and ungerade parity of the wave function interfere [4]. For this interference to happen the electrons have to be indistinguishable and hence energetically degenerate. If this is the case one can end up with a coherent superposition of a core-hole state with gerade and ungerade symmetries, where the relative phase between the outgoing electron waves determines if the core-hole density is more localized on the left or the right carbon atoms. As a consequence it would be conceivable that the C-H bond closer to the hole is more likely to break. While the electron g-u core-hole states are indistinguishable during the fast Auger decay (g-u splitting is about 20 meV, Auger decay time is ~5 fs), the MFAAD in Fig. 4 does not support such a scenario because it does not show any asymmetry. The reasons for that can be that either only g or u states are populated or that the outer valence electrons redistribute so fast that the memory of where the second electron was ejected from is lost before the proton is expelled. By all means, we see no link between the direction of the Auger electron and the bond breaking for the deprotonation channel, a fact that will be different for a special case of the symmetric breakup of the ethylene molecule (see below).

In conclusion we cannot report any fine structure or asymmetry based on interference due to diffraction or core-hole localization for either features of the deprotonation channel.

2. $CH_2{}^+ + CH_2{}^+$ *channel*

The MFAADs presented here for the symmetric breakup (Fig. 5) exhibit much more distinct structures than in the deprotonation channel shown in Fig. 4. This is likely due to the fact that the fragmentation along the central C=C bond reflects the orientation of the molecule at the time of the double ionization much more accurately. The Auger electron angular distribution, corresponding to the main feature ($254 < \mathrm{KER} + E_{\mathrm{Auger}} < 263$ eV) in the energy correlation map of the symmetric channel [island (I) in Fig. 1(b)], exhibits four broad lobes along 50° [see Fig. 5(a)]. At first glance it seems conceivable that electronic states resulting from the removal of both σ- and π-type orbitals contribute to the fragmentation pathways, since the contribution along and perpendicular to the molecular axis is nonzero. From the energetics we have identified the following states of the dication [see Fig. 2(b)] to be the most likely candidates [29]: ${}^1B_{3u} \rightarrow [3a_g^{-1}, 1b_{3u}^{-1}]$ in which one electron is ejected from a σ orbital and the other one from a π orbital, ${}^1B_{3g} \rightarrow [3a_g^{-1}, 1b_{3g}^{-1}]$, i.e., both electrons are emitted from σ orbitals, and subsequently ${}^1B_{1g} \rightarrow [1b_{2u}^{-1}, 1b_{3u}^{-1}]$ as well as ${}^1B_{2g} \rightarrow [2b_{1u}^{-1}, 1b_{3u}^{-1}]$, where in both cases one

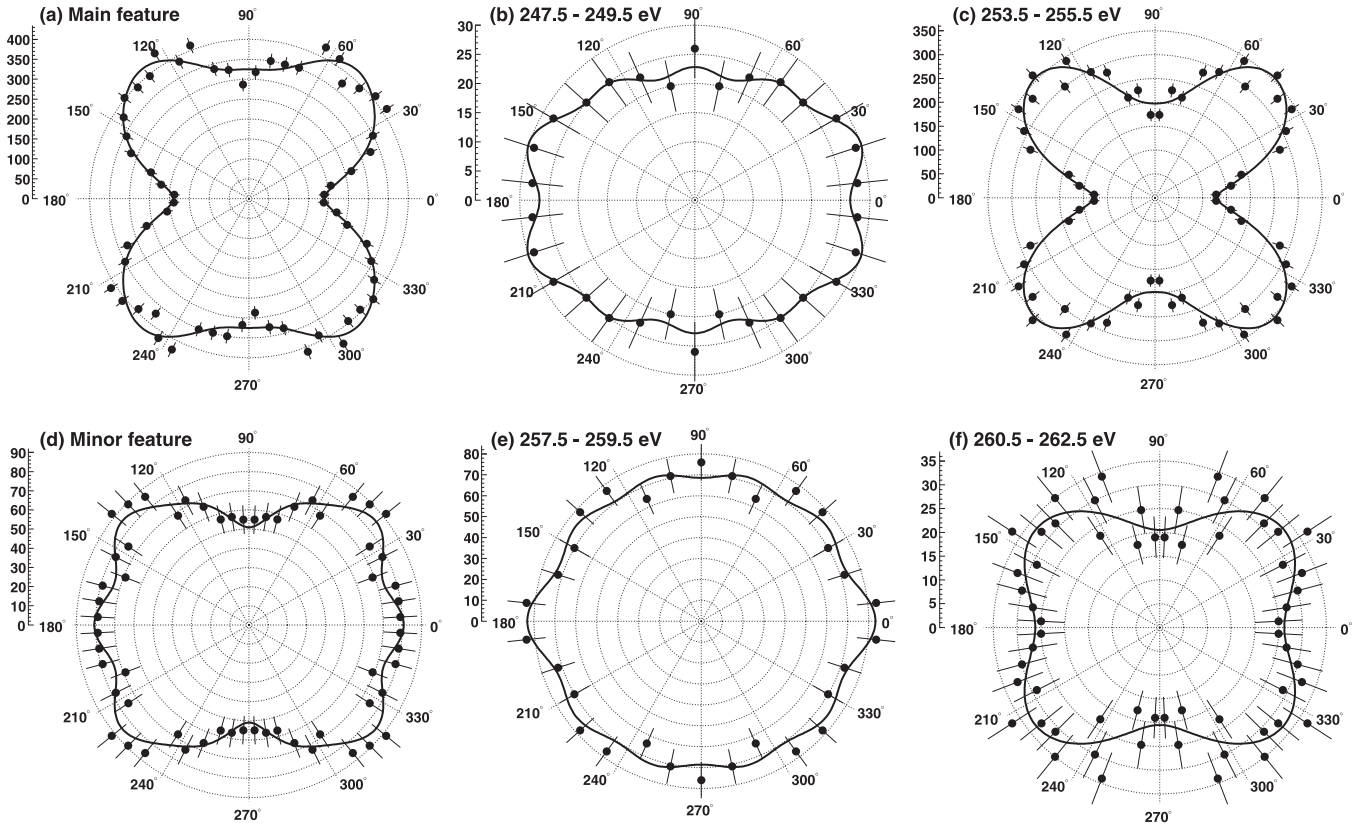

FIG. 5. Auger electron angular distributions for two different features (a, d) and four different Auger electron energies E_{Auger} intervals (b, c, e, f) of the symmetric breakup channel in Fig. 1(b): (a) main feature I, (b) $E_{\text{Auger}} = 247.5-249.5\,\text{eV}$, (c) $E_{\text{Auger}} = 253.5-255.5\,\text{eV}$, (d) minor feature II, (e) $E_{\text{Auger}} = 257.5-259.5\,\text{eV}$, and (f) $E_{\text{Auger}} = 260.5-262.5\,\text{eV}$. For the fitting with spherical harmonics (lines) $l = 0-4$ and $m = 0$ are used. The molecular axis is horizontal and the plane of the figure represents the polarization plane of the circular polarized light.

electron is ejected from a σ orbital while the other one originates from a π orbital [31].

The angular distribution of the minor feature, i.e., the feature at higher E_{Auger} ($264 < \text{KER} + E_{\text{Auger}} < 271\,\text{eV}$) in Fig. 1(b) [island (II)], shown in Fig. 5(d), differs from the four-leaf-clover shape of the main feature. While it still preserves the small dip perpendicular to the molecular axis, it suggests having an increased Auger emission from σ-type orbitals. This would imply that the unoccupied virtual orbitals of σ type, namely $3b_{1u}$, $2b_{2u}$, $4a_g$, and $2b_{3g}$, are responsible for this increased contribution along the molecular axis resulting in the change in shape. The Auger emission from these virtual orbitals is in accordance with the observed E_{Auger} in energy correlation maps from Fig. 1(b).

On the other hand, a d-like angular momentum shape in terms of spherical harmonics, as we show it in Fig. 5(a), tells us that the MFAAD is likely not caused by simply adding distributions along and perpendicular to the molecular axis, stemming from emissions from σ and π orbitals, respectively. If this would be the case, we would expect an isotropiclike pattern $(|A_1 \sin^2\phi| + |A_2 \cos^2\phi|$, where A_1 and A_2 are amplitudes of similar value), i.e., no nodes in the electron angular distribution along or perpendicular to the molecular axis. However, the higher angular momentum found here in the fits with spherical harmonics of the MFAADs can be reproduced by the coherent sum of p waves $(|B_1 \sin\phi| + |B_2 \cos\phi|)^2$ emitted perpendicular to and along the molecular orientation (not shown here) and hence suggests that the observed MFAADs are mainly caused by multiple scattering of the outgoing Auger electron wave in the molecular potential. This seems plausible since contributions from higher angular momentum in the scattering process of the Auger electron were found in small molecules before (such as N_2 and CO [4,47,48,56]).

The symmetric breakup channel with its good statistics and the ability to track back the molecular orientation at the time of the photoabsorption enables us to investigate the MFAADs for the main and minor features in more detail. In Figs. 5(b), 5(c), 5(e), and 5(f) we present the MFAADs for selected Auger electron energies and a common KER between 4.5 and 7 eV [see Fig. 1(b)]. The angular distributions clearly vary within the 2-eV steps of the Auger electron energy. It appears that at least four different states can now be distinguished while both the main and the minor features, presented in Figs. 5(a) and 5(d) above, were just showing the MFAADs averaged over the broad E_{Auger} intervals selected in Fig. 1(b). This indicates that the ejected electron originates from different orbitals [57].

The Auger electron angular distribution for the islandlike feature in the energy map of the symmetric breakup channel [island (III) in Fig. 1(b)] is shown in Fig. 6(a). It is apparently quite different from the other two features discussed above. The distribution is highly structured and seems to require an explanation beyond the multiple scattering approach used to understand the MFAADs in Fig. 5, since the fit with spherical

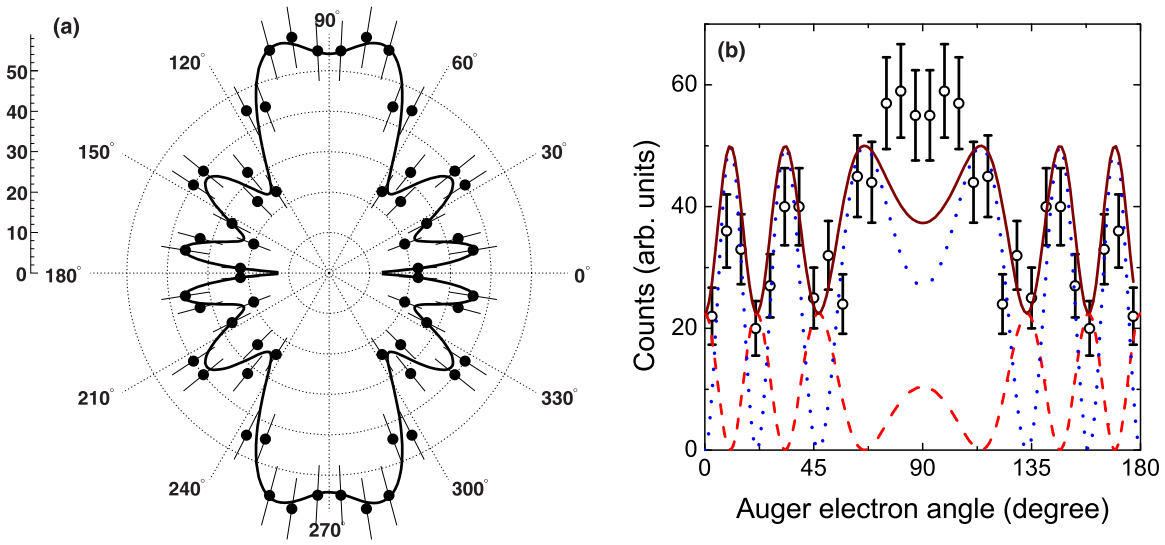

FIG. 6. (Color online) Molecular frame Auger electron angular distribution for the islandlike feature of the symmetric breakup channel [feature III in Fig. 1(b)]. For the fitting with spherical harmonics (line) in (a) $l = 0 - 4$ and $m = 0$, and ± 1 are needed. The circles in (b) represent the measured data while the dashed and dotted lines represent the cosine and sine functions of the diffraction patterns of the Auger electrons from g and u states. The solid line represents the incoherent sum of both contributions. The molecular axis is horizontal and the plane of the figure represents the polarization plane of the circular polarized light.

harmonics requires $m = \pm 1$, i.e., partial waves with different symmetries. While in Fig. 5 it was sufficient to think of the Auger electron as being emitted from one single electronic state undergoing multiple scattering and consequently showing a diffraction pattern, this approach fails for the islandlike feature; it seems that multiple (degenerate) states are involved. The questions arise: Where does this highly distinct structure come from and why does it exclusively show up for this very localized feature in the energy correlation map?

Let us look at the energies first: Superficially, the energies on the PES for this feature only include the first excited electronic state $^1A_u(S_2) \rightarrow [1b_{3g}^{-1}, 1b_{3u}^{-1}]$ of the dication, which corresponds to the removal of electrons from σ and π orbitals. At first glance this seems plausible since the main lobe perpendicular to the molecular axis can be considered a signature of the state resulting from removal of a π-orbital electron and hence nicely confirms the dominating population of the S_2 state. However, in the case of the islandlike feature [island (III) in Fig. 1(b)] no repulsive curve is directly populated on the PES, but instead the molecule dissociates while going through conical intersections that coincide with our narrow energy window on the PES as outlined above. From the energies we know that these rare events observed here stem from a select few neutral molecules, which were doubly ionized in the vicinity of the conical intersections $S_3 - S_2$ (i.e., between the S_3 and S_2 states) and $S_2 - S_1$ (i.e., between the S_2 and S_1 states). This stack of funnels is characterized by the S_1 and S_3 states approaching the PES of S_2(see Table III and Fig. 10(d) in [31]). For the S_1 state this is realized by a small fraction of molecules with a torsion angle close to zero; for those configurations the otherwise umbrellalike PES forms a sharp cusp touching S_2. For the S_3 state the C-C bond length shrinks, while the C-H distance elongates and the H-C-H angles get smaller. This is not reflected in Fig. 2(b), which only shows a cut of the PESs offside the conical intersection. At these funnels not only the conformation such as the torsion mode along the C-C bond changes but also the energies of the electronic states S_1, S_2, and S_3 become degenerate; they cannot be distinguished anymore. From the orbitals involved, as discussed above, we can deduce that the Auger electrons from the S_1 and S_2 states are likely of ungerade parity, while the Auger electron from the S_3 state is of gerade symmetry. Since these Auger electrons are energetically degenerate, as facilitated by the conical intersections, the observed MFAAD is likely caused by the sum of diffraction patterns from one g and two u states.

We want to support this finding by taking a closer look at the MFAAD: The photoionization took place near a shape resonance. Highly differential measurements have revealed an "f-wave shape resonance" near threshold (298 eV) for the core ionization of C_2H_4 [52]. In our present measurement we have used 310-eV photons; i.e., we are at the tail of this shape resonance. Here the mix of gerade and ungerade photoelectrons is expected to be different from 50 : 50. In Fig. 6(b), we fitted the incoherent sum of diffraction patterns from Auger electrons (258 eV) of gerade and ungerade symmetry by varying the respective amplitudes and keeping the common internuclear distance constant. We find a good agreement with the experimental data for a g-u mix of about 1:2, which is close to the numbers of g and u orbitals involved (as explained above) and a short distance of 2.0 a.u. which reflects the C=C shortening in the S_3 state.

We note that different amounts of g and u states of the ethylene dication become degenerate while going through the two conical intersections. The unequal contribution from gerade and ungerade Auger electrons results in the observed mix of diffraction patterns in Fig. 6(a). This phenomenon actually gives rise to the possibility of photoelectron–Auger electron entanglement when considering the parity of the corresponding photoelectron and recoiling $C_2H_4^{2+}$ ion: We

know that the dication dissociates on the S_1 state, which is of gerade symmetry. Moreover, as mentioned above, the *g*-*u* splitting of the neutral ground state C_2H_4 molecule is only 0.02 eV, while the Auger decay happens within ~5 fs, resulting in an energy width that is broader than the partition between the *g* and *u* states. Therefore we can expect a mix of contributions from the gerade and ungerade state for the photoelectrons as well. Considering these facts, the Auger electron angular distribution found in Fig. 6(a) parallels the emission pattern of the Auger electrons in the *K*-shell photoionization of molecular nitrogen [4]; the Auger electrons are entangled with the photoelectrons. As in the case of N_2, the MFAAD ostensibly shows the incoherent sum of the contributions (i.e., diffraction patterns) from orbitals with gerade and ungerade symmetry of the dication state or, alternatively speaking, a superposition of states corresponding to a core hole on one or the other carbon atom of the centrosymmetric molecule.

The entanglement of photoelectrons and Auger electrons is based on parity conservation. The neutral ethylene ground state is of gerade symmetry and with one single photon of ungerade symmetry double ionizing the molecule, the overall product consisting of a photoelectron, an Auger electron, and a dication, has to be ungerade. The S_1 dication state leading to dissociation after the molecule funneled through the conical intersections is of gerade parity. Hence the joint wave function of Auger electron and photoelectron is a Bell-type state where the two-electron wave function is the sum of the Auger electron gerade–photoelectron ungerade product and Auger electron ungerade–photoelectron gerade product $\langle\Psi_f^{++}\psi_{\mathbf{k}_A}^-|V|\Psi_{\sigma_g}^+\rangle\langle\Psi_{\sigma_g}^+\psi_{\mathbf{k}_p}^-|d|\Psi_0\rangle + \langle\Psi_f^{++}\psi_{\mathbf{k}_A}^-|V|\Psi_{\sigma_u}^+\rangle\langle\Psi_{\sigma_u}^+\psi_{\mathbf{k}_p}^-|d|\Psi_0\rangle$ in order to conserve the parity. Here, $\langle\Psi_{1\sigma_{g,u}}^+\psi_{\mathbf{k}_p}^-|d|\Psi_0\rangle$ is the dipole amplitude describing the photoionization and $\langle\Psi_f^{++}\psi_{\mathbf{k}_A}^-|V|\Psi_{1\sigma_{g,u}}^+\rangle$ is the Coulomb matrix element representing the subsequent Auger decay (taken from Ref. [4]). The initial neutral state of the ethylene molecule is described by Ψ_0, $\Psi_{1\sigma_{g,u}}^+$ is the intermediate (gerade or ungerade) state of the singly ionized ethylene molecule, and Ψ_f^{++} is the final state of the dication.

To prove this experimentally a coincident measurement between the entangled photoelectron, Auger electron, and the recoiling ions is necessary—the angular distributions of the photo or Auger electrons alone are not sufficient to verify this entanglement; they by themselves just show the result of an incoherent sum of *g* and *u* contributions [as outlined in Fig. 6(b) for the Auger electron]. In case of a coincidence measurement the angular distribution of the Auger electrons of the islandlike feature would then allow for breaking the symmetry of the Auger electron angular emission pattern. The latter would happen if, for the given dication state with gerade parity, the entangled photoelectron could be selected as a superposition of gerade and ungerade symmetry forcing the Auger electron to have the reverse *g*-*u* mix, which would be able to produce an asymmetric MFAAD as demonstrated in [4]. In this case the angular distributions have to be described as the coherent sum of *g* and *u* states. Unfortunately the yield of this particular pathway [i.e., island (III) in Fig. 1(b)] leading to the symmetric fragmentation is very low [see Table I: island (III)] and thus hard to detect with any significant statistics. Moreover, in our present measurements we only detected the Auger electron in coincidence with the recoiling ions while we repel the photoelectrons.

Apparently the axial recoil approximation still seems to hold while going through the conical intersections. This is likely because the Auger decay happens on the same ultrafast time scale of the nuclear dynamics in the vicinity of the conical intersections, and the torsion around the C-C axis as well as its bond contraction does not significantly change the orientation of the molecule during the fragmentation.

In conclusion, we interpret the highly structured MFAAD of the islandlike feature (not as a proof but) as a fingerprint of the entangled photoelectron–Auger electron pair, comparable to the case of N_2. The two conical intersections S_3-S_2 and S_2-S_1, which are practically on top of each other, lead to a mix of *g* and *u* Auger electron states and non–Born-Oppenheimer behavior where electrons and ions move on the same time scales. As outlined in Ref. [31], the molecule undergoes a substantial conformation change in this course of events. In case the entanglement can be verified (for instance, in a coincidence measurement as described above), the strong correlation between the photoelectron and Auger electron apparently seems to survive during the concerted motion of this photochemical process, a fact not evident in diatomic molecules such as N_2 because of the absence of conical intersections on the PESs.

3. $H_2^+ + C_2H_2^+$ *channel*

The Auger electron angular distribution for the molecular hydrogen ion elimination channel is shown in Fig. 7. For the main feature ($252 < \mathrm{KER} + E_{\mathrm{Auger}} < 262$ eV) in the energy correlation map of Fig. 1(c) [island (I)] the distribution is nearly isotropic [see Fig. 7(a)]. This could again mean that states which result from the removal of electrons from both σ and π orbitals contribute to this fragmentation channel almost equally. In particular, the Auger decay results in the population of the following dicationic states: $^1B_{1u} \rightarrow [1b_{2u}^{-1}, 1b_{3g}^{-1}]$, where both electrons were ejected from a σ orbital, or $[1b_{3g}^{-2}, 1b_{3u}^{-1}, 1b_{2g}^{+1}]$, i.e., an emission in which two electrons originated from a σ orbital and one from a π orbital while one of them occupied the π^* orbital. Other candidates are the state $^1B_{2u} \rightarrow [1b_{2u}^{-1}, 3a_g^{-1}]$, where both electrons were ejected from σ orbitals, and the state $^1B_{2g} \rightarrow [2b_{1u}^{-1}, 1b_{3u}^{-1}]$ that has one electron removed from a σ orbital and the other from a π orbital. Another likely state is represented by $^1A_g(S_4) \rightarrow [3a_g^{-2}]$, which results from removing both electrons from σ orbitals. The sum of all these populated states represents an almost uniform mix of σ and π orbitals in accordance with the observed nearly isotropic Auger electron angular distribution. In the case of the molecular hydrogen ion H_2^+ is formed by hydrogen atoms bound to the same carbon; no direct repulsive PES is found along the $C-H_2$ coordinate, but instead a barrier prevents this dissociation. In order to fragment, the dication has to undergo a conformation change in the H-C-H angle coordinate. The dication reduces this angle while lowering the energy on the PES and simultaneously circumvents the barrier present in the $C-H_2$ coordinate [29]. It then finally finds the repulsive state to dissociate into H_2^+ and $C_2H_2^+$ fragments. However, the observed near-isotropic angular distribution contradicts this scenario as we expect to

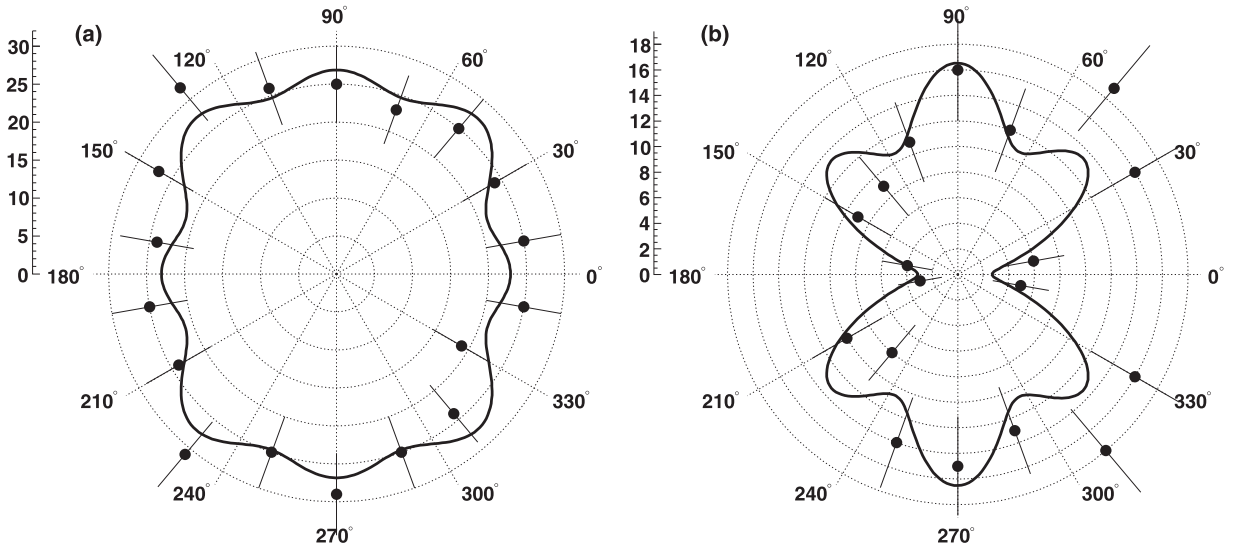

FIG. 7. Auger electron angular distribution for the molecular hydrogen ion elimination channel after K-shell ionization of C_2H_4. For the fitting of (a) and (b) with spherical harmonics (lines), $l = 0-4$ and $m = 0$ only are used. The molecular hydrogen ion $H_2{}^+$ goes to the right and the plane of the figure represents the polarization plane of the circular polarized light.

see a break in symmetry of the MFAAD. Instead it suggests that the two hydrogen atoms were bound to different carbon atoms before they come closer to form the molecular hydrogen ion. The latter process involves the migration of the proton along the double bond and convolutes the orientation of the molecular axis, and hence smears the angular distribution of the Auger electron. We cannot discern between the two possible outcomes because the mass to charge ratio for acetylene (H−C=C−H) -like and vinylidene (C=C<HH) -like fragments are the same. This investigation could be improved by picking an isomer such as partially deuterated ethylene (HH > C=C < DD,) to better track this dissociation channel of the molecule in the future.

The minor feature corresponding to the higher E_{Auger} region ($262 < \text{KER} + E_{\text{Auger}} < 271$ eV) in the energy correlation map [island (II) in Fig. 1(c)] has a different-looking angular distribution compared to the major feature and is displayed in Fig. 7(b). This distribution is dominated by an emission perpendicular to the molecular axis, an indication of a preferred emission from π-type orbitals. This scenario is unlike the deprotonation channel described earlier, where both the main and minor features have about the same angular distribution (see Fig. 4). The states responsible for this minor feature in the molecular hydrogen ion elimination channel involve emissions of electrons from virtual orbitals. The electron is excited to the π^* orbital and ejected when the Auger decay involves an inner valence electron (instead of an outer valence). The small yield of this particular breakup channel points to either the shake-up satellite (SA) or the conjugate (CA) process as the underlying mechanism of double ionization. The very low statistics prevents us from further investigating this interesting channel.

IV. SUMMARY

Exploiting our coincident recoil-ion and Auger electron 3D-momentum imaging scheme we were able to probe the multi-dimensional potential energy surfaces of the ethylene dication after K-shell ionization followed by subsequent Auger decay. The PIPICO spectra helped us to distinguish three different fragmentation channels (deprotonation, symmetric breakup, and molecular hydrogen ion elimination). The (corrected) branching ratios allowed us to classify the most probable double ionization decay mechanisms. The main feature in the fragmentation of all three dissociation channels is the result of the normal or direct Auger (DA) process. The minor features likely stem from a mix of the shake-up-like satellite states (SA) and the conjugate (CA) processes involving virtual orbitals.

Energy correlation maps representing the kinetic energies of the Auger electrons as a function of the KER in combination with the PESs from our multiconfiguration self-consistent field method enabled us to identify the most likely electronic states involved in the fragmentation pathways. For almost all transitions it sufficed to take singlet states into account. We found progression of vibrational bound states that dissociate on repulsive curves while, on the other hand, transitions via hidden crossings and conical intersections were observed.

Furthermore, our measured molecular frame Auger electron angular distributions support the assignment of the electronic dicationic states and often reflect the symmetry of the orbitals the Auger electrons were emitted from. We found no hints of core-hole localization or diffraction in the deprotonation channel; all MFAADs showed a symmetric emission pattern. However, in the case of the symmetric channel, we find strong evidence of multiple scattering of the outgoing Auger electron. The additional islandlike feature at low KER in the energy correlation map displays a highly structured angular distribution similar to the Auger decay of N_2. This, in combination with the localized island in the electron-ion energy map, the small $g-u$ splitting of the ethylene ground state, and the gerade symmetry of the dissociating dication, suggests an entangled Auger

and photoelectron pair. The conical intersections between the two excited states and the ground states (i.e., S_3-S_2 and S_2-S_1) result in degenerate electronic states which give rise to the mix of interference patterns of Auger electrons emitted from gerade and ungerade orbitals, while the molecule undergoes strong non–Born-Oppenheimer behavior (ultrafast shrinking, scissoring, and torsion) on the scale of the Auger decay time. The K-shell ionization of ethylene represents a great candidate for investigating electron entanglement and core-hole localization for the symmetric breakup of this polyatomic molecule if Auger electrons and photoelectrons could be measured in coincidence. It would be beneficial if theoretical studies could provide more information on these features observed in the present study.

ACKNOWLEDGMENTS

This research used the Advance Light Source and resources of the National Energy Research Scientific Computing Center, DOE Offices of Science User Facilities supported by the Director, Office of Science, Office of Basic Energy Sciences, the Division of Chemical Sciences, Geosciences, and Biosciences of the U.S. Department of Energy at LBNL under Contract No. DE-AC02-05CH11231. We thank the staff of the Advanced Light Source, in particular beamline 11.0.2 scientists H. Bluhm and T. Tyliszczak for their outstanding support. JRML personnel were supported by Grant No. DE-FG02-86ER13491 from the same funding agency. We acknowledge the financial support of the Deutsche Akademische Austausch Dienst (DAAD) and the Deutsche Forschungs Gemeinschaft (DFG).

[1] J. S. Briggs and V. Schmidt, J. Phys. B **33**, R1 (2000).
[2] D. Akoury, K. Kreidi, T. Jahnke, Th. Weber, A. Staudte, M. Schöffler, N. Neumann, J. Titze, L. Ph. H. Schmidt, A. Czasch, O. Jagutzki, R. A. Costa Fraga, R. E. Grisenti, R. Díez Muiño, N. A. Cherepkov, S. K. Semenov, P. Ranitovic, C. L. Cocke, T. Osipov, H. Adaniya *et al.*,Science **318**, 949 (2007).
[3] N. Chandra and R. Ghosh, Phys. Rev. A **69**, 012315 (2004).
[4] M. S. Schöffler, J. Titze, N. Petridis, T. Jahnke, K. Cole, L. P. H. Schmidt, A. Czasch, D. Akoury, O. Jagutzki, J. B. Williams *et al.*, Science **320**, 920 (2008).
[5] S. Hsieh and J. H. D. Eland, J. Phys. B **29**, 5795 (1996).
[6] P. Lablanquie, J. H. D. Eland, I. Nenner, P. Morin, J. Delwiche, and M. J. Hubin-Franskin, Phys. Rev. Lett. **58**, 992 (1987).
[7] J. H. D. Eland, S. D. Price, J. C. Cheney, P. Lablanquie, I. Nenner, and P. G. Fournier, Philos. Trans. R. Soc., A **324**, 247 (1988).
[8] T. Åberg, Phys. Rev. A **2**, 1726 (1970).
[9] T. Schneider, P. L. Chocian, and J.-M. Rost, Phys. Rev. Lett. **89**, 073002 (2002).
[10] T. Y. Shi and C. D. Lin, Phys. Rev. Lett. **89**, 163202 (2002).
[11] J. Viefhaus, L. Avaldi, G. Snell, M. Wiedenhöft, R. Hentges, A. Rüdel, F. Schäfers, D. Menke, U. Heinzmann, A. Engelns, J. Berakdar, H. Klar, and U. Becker, Phys. Rev. Lett. **77**, 3975 (1996).
[12] T. Weber, A. O. Czasch, O. Jagutzki, A. K. Müller, V. Mergel, A. Kheifets, E. Rotenberg, G. Meigs, M. H. Prior, S. Daveau *et al.*, Nature **431**, 437 (2004).
[13] T. Weber, A. Czasch, O. Jagutzki, A. Müller, V. Mergel, A. Kheifets, J. Feagin, E. Rotenberg, G. Meigs, M. H. Prior, A. Landers, C. L. Cocke, T. Osipov, R. Díez Muiño, H. Schmidt-Böcking, and R. Dörner, Phys. Rev. Lett. **92**, 163001 (2004).
[14] M. Gisselbrecht, M. Lavollée, A. Huetz, P. Bolognesi, L. Avaldi, D. P. Seccombe, and T. J. Reddish, Phys. Rev. Lett. **96**, 153002 (2006).
[15] P. Bolognesi, B. Joulakian, A. A. Bulychev, O. Chuluunbaatar, and L. Avaldi, Phys. Rev. A **89**, 053405 (2014).
[16] A. A. Bulychev, O. Chuluunbaatar, A. A. Gusev, and B. Joulakian, J. Phys. B **46**, 185203 (2013).
[17] U. Becker, O. Hemmers, B. Langer, A. Menzel, R. Wehlitz, and W. B. Peatman, Phys. Rev. A **45**, R1295 (1992).
[18] S. D. Price and J. H. D. Eland, J. Phys. B **24**, 4379 (1991).
[19] R. Feifel, J. H. D. Eland, and D. Edvardsson, J. Chem. Phys. **122**, 144308 (2005).
[20] X.-J. Liu, Q. Miao, F. Gel'mukhanov, M. Patanen, O. Travnikova, C. Nicolas, H. Ågren, K. Ueda, and C. Miron, Nat. Photonics **9**, 120 (2015).
[21] A. E. Slattery, T. A. Field, M. Ahmad, R. I. Hall, J. Lambourne, F. Penent, P. Lablanquie, and J. H. D. Eland, J. Chem. Phys. **122**, 084317 (2005).
[22] T. Masuoka, E. Nakamura, and A. Hiraya, J. Chem. Phys. **104**, 6200 (1996).
[23] P. Morin, M. Simon, C. Miron, N. Leclercq, E. Kukk, J. D. Bozek, and N. Berrah, Phys. Rev. A **61**, 050701(R) (2000).
[24] D. Céolin, C. Miron, M. Simon, and P. Morin, J. Electron Spectrosc. Relat. Phenom. **141**, 171 (2004).
[25] H. Sann, T. Jahnke, T. Havermeier, K. Kreidi, C. Stuck, M. Meckel, M. S. Schöffler, N. Neumann, R. Wallauer, S. Voss, A. Czasch, O. Jagutzki, Th. Weber, H. Schmidt-Böcking, S. Miyabe, D. J. Haxton, A. E. Orel, T. N. Rescigno, and R. Dörner, Phys. Rev. Lett. **106**, 133001 (2011).
[26] S. Truong, A. Yencha, A. Juarez, S. Cavanagh, P. Bolognesi, and G. King, Chem. Phys. Lett. **474**, 41 (2009).
[27] J. H. D. Eland, Chem. Phys. **294**, 171 (2003).
[28] J. H. D. Eland, Chem. Phys. **323**, 391 (2006).
[29] B. Gaire, S. Y. Lee, D. J. Haxton, P. M. Pelz, I. Bocharova, F. P. Sturm, N. Gehrken, M. Honig, M. Pitzer, D. Metz, H.-K. Kim, M. Schöffler, R. Dörner, H. Gassert, S. Zeller, J. Voigtsberger, W. Cao, M. Zohrabi, J. Williams, A. Gatton *et al.*, Phys. Rev. A **89**, 013403 (2014).
[30] O. Travnikova, V. Kimberg, R. Flammini, X-J Liu, M. Patanen, C. Nicolas, S. Svensson, and C. Miron, J. Phys. Chem. Lett. **4**, 2361 (2013).
[31] E. Ohrendorf, H. Köppel, L. S. Cederbaum, F. Tarantelli, and A. Sgamellotti, J. Chem. Phys. **91**, 1734 (1989).
[32] T. Osipov, C. L. Cocke, M. H. Prior, A. Landers, Th. Weber, O. Jagutzki, L. Schmidt, H. Schmidt-Böcking, and R. Dörner, Phys. Rev. Lett. **90**, 233002 (2003).
[33] J. van Tilborg, T. K. Allison, T. W. Wright, M. P. Hertlein, R. W. Falcone, Y. Liu, H. Merdji, and A. Belkacem, J. Phys. B **42**, 081002 (2009).
[34] R. Fink, S. Sorensen, A. de Brito, A. Ausmees, and S. Svensson, J. Chem. Phys. **112**, 6666 (2000).

[35] H. Beckmann, W. Braun, H. Jochims, E. Ruhl, and H. Baumgartel, Chem. Phys. Lett. **121**, 499 (1985).
[36] L. J. Medhurst, T. A. Ferrett, P. A. Heimann, D. W. Lindle, S. H. Liu, and D. A. Shirley, J. Chem. Phys. **89**, 6096 (1988).
[37] K. Kuramoto, M. Ehara, and H. Nakatsuji, J. Chem. Phys. **122**, 014304 (2005).
[38] B. H. Bransden and C. J. Joachain, *Physics of Atoms and Molecules*, 2nd ed. (Pearson Education Ltd, Harlow, UK, 2003).
[39] B. Kempgens, A. Kivimäki, B. S. Itchkawitz, H. M. Köppe, M. Schmidbauer, M. Neeb, K. Maier, J. Feldhaus, and A. M. Bradshaw, J. Electron Spectrosc. Relat. Phenom. **93**, 39 (1998).
[40] T. Jahnke, J. Titze, L. Foucar, R. Wallauer, T. Osipov, E. P. Benis, O. Jagutzki, W. Arnold, A. Czasch, A. Staudte, M. Schöffler, A. Alnaser, T. Weber, M. H. Prior, H. Schmidt-Böcking, and R. Dörner, J. Electron Spectrosc. Relat. Phenom. **183**, 48 (2011).
[41] A. J. Menssen, C. S. Trevisan, M. S. Schöffler, A. Gatton, J. Sartor, M. Zohrabi, B. Berry, B. Gaire, F. Trinter, A. Belkacem, T. Jahnke, R. Dörner, A. L. Landers, C. W. McCurdy, T. N. Rescigno, Th. Weber, and J. B. Williams (unpublished).
[42] C. E. Liekhus-Schmaltz, I. Tenney, T. Osipov, A. Sanchez-Gonzalez, N. Berrah, R. Boll, C. Bomme, C. Bostedt, J. D. Bozek, S. Carron, R. Coffee, J. Devin, B. Erk, K. R. Ferguson, R. W. Field, L. Foucar, L. J. Frasinski, J. M. Glownia, M. Gühr *et al.* (unpublished).
[43] N. A. Cherepkov, S. K. Semenov, M. S. Schöffler, J. Titze, N. Petridis, T. Jahnke, K. Cole, L. Ph. H. Schmidt, A. Czasch, D. Akoury, O. Jagutzki, J. B. Williams, T. Osipov, S. Lee, M. H. Prior, A. Belkacem, A. L. Landers, H. Schmidt-Böcking, R. Dörner, and Th. Weber, Phys. Rev. A **82**, 023420 (2010).
[44] F. P. Sturm, M. Schöffler, S. Lee, T. Osipov, N. Neumann, H.-K. Kim, S. Kirschner, B. Rudek, J. B. Williams, J. D. Daughhetee, C. L. Cocke, K. Ueda, A. L. Landers, Th. Weber, M. H. Prior, A. Belkacem, and R. Dörner, Phys. Rev. A **80**, 032506 (2009).
[45] H. Ågren and O. Vahtras, J. Phys. B **26**, 913 (1993).
[46] T. Kerkau and V. Schmidt, J. Phys. B **34**, 839 (2001).
[47] T. Weber, M. Weckenbrock, M. Balser, L. Schmidt, O. Jagutzki, W. Arnold, O. Hohn, M. Schöffler, E. Arenholz, T. Young, T. Osipov, L. Foucar, A. De Fanis, R. Díez Muiño, H. Schmidt-Böcking, C. L. Cocke, M. H. Prior, and R. Dörner, Phys. Rev. Lett. **90**, 153003 (2003).
[48] N. A. Cherepkov, S. K. Semenov, M. S. Schöffler, J. Titze, N. Petridis, T. Jahnke, K. Cole, L. Ph. H. Schmidt, A. Czasch, D. Akoury, O. Jagutzki, J. B. Williams, C. L. Cocke, T. Osipov, S. Lee, M. H. Prior, A. Belkacem, A. L. Landers, H. Schmidt-Böcking, Th. Weber *et al.*, Phys. Rev. A **80**, 051404(R) (2009).
[49] R. Dörner, V. Mergel, O. Jagutzki, L. Spielberger, J. Ullrich, R. Moshammer, and H. Schmidt-Böcking, Phys. Rep. **330**, 95 (2000).
[50] J. Ullrich, R. Moshammer, A. Dorn, R. Dörner, L. P. H. Schmidt, and H. Schmidt-Böcking, Rep. Prog. Phys. **66**, 1463 (2003).
[51] T. Jahnke, T. Weber, T. Osipov, A. L. Landers, O. Jagutzki, L. P. H. Schmidt, C. L. Cocke, M. H. Prior, H. Schmidt-Böcking, and R. Dörner, J. Electron Spectrosc. Relat. Phenom. **141**, 229 (2004).
[52] T. Osipov, M. Stener, A. Belkacem, M. Schöffler, T. Weber, L. Schmidt, A. Landers, M. H. Prior, R. Dörner, and C. L. Cocke, Phys. Rev. A **81**, 033429 (2010).
[53] R. R. Rye, T. E. Madey, J. E. Houston, and P. H. Holloway, J. Chem. Phys. **69**, 1504 (1978).
[54] M. Thompson, P. A. Hewitt, and D. S. Woolscroft, Anal. Chem. **48**, 1336 (1976).
[55] E. Y. Sidky and I. Ben-Itzhak, Phys. Rev. A **60**, 3586 (1999).
[56] A. V. Golovin, J. Adachi, S. Motoki, M. Takahashi, and A. Yagishita, J. Phys. B **38**, L63 (2005).
[57] K. Zähringer, H.-D. Meyer, and L. S. Cederbaum, Phys. Rev. A **46**, 5643 (1992).